INSTITUTE OF PHYSICS PUBLISHING JOURNAL OF PHYSICS: CONDENSED MATTER

J. Phys.: Condens. Matter **17** (2005) S1329–S1338 doi:10.1088/0953-8984/17/16/004

NanoESCA: a novel energy filter for imaging x-ray photoemission spectrosocpy

M Escher[1], N Weber[1], M Merkel[1], C Ziethen[2], P Bernhard[2], G Schönhense[2], S Schmidt[3], F Forster[3], F Reinert[3], B Krömker[4] and D Funnemann[4]

[1] Focus GmbH, 65510 Hünstetten, Germany
[2] Johannes Gutenberg Universität Mainz, Institut für Physik, 55099 Mainz, Germany
[3] Universität des Saarlandes, FR 7.2. Experimentalphysik, 66041 Saarbrücken, Germany
[4] Omicron NanoTechnology GmbH, 65232 Taunusstein, Germany

E-mail: m.escher@focus-gmbh.com

Received 13 May 2004, in final form 9 December 2004
Published 8 April 2005
Online at stacks.iop.org/JPhysCM/17/S1329

Abstract
A novel instrument for imaging ESCA is described. It is based on a tandem arrangement of two hemispherical energy analysers used as an imaging energy filter. The main spherical aberration (α^2-term) of the analyser is corrected by the antisymmetry of the tandem configuration. The kinetic energy range useable for imaging extends up to 1.6 keV; this is compatible with Mg and Al Kα laboratory x-ray sources. First experiments on the chemical surface composition of a $Cu_{0.98}Bi_{0.02}$ polycrystal, a GaAs/AlGaAs heterostructure and Ag crystallites on Si(111) have been performed using synchrotron radiation. The results reveal an energy resolution of 190 meV and a lateral resolution (edge resolution) of 120 nm. Besides elimination of the analyser's spherical aberration, the tandem arrangement largely retains the time structure of the electron signal, unlike a single hemispherical analyser.

(Some figures in this article are in colour only in the electronic version)

1. Introduction

The worldwide advances in nanoscience and nanotechnology have strongly pushed the development and improvement of adequate analytical methods. In the field of microscopy there has been dramatic progress in imaging performance. Today scanning tunnelling microscopy (STM) is a standard tool for imaging of conducting surfaces with atomic resolution. Modern transmission electron microscopy (TEM) also provides atomic resolution,

© 2005 IOP Publishing Ltd Printed in the UK

and aberration correction [1] paves the way to 'sub-Å resolution' in the future [2]. Less progress has been achieved in the field of nanospectroscopy. X-ray fluorescence (EDX) or Auger microprobes in scanning electron microscopy reached their principal limits several years ago. Their lateral and depth resolution is limited by electron scattering processes (blooming) within the surface region of the sample. Further restrictions are the low x-ray fluorescence yield and the low signal-to-background ratio of electron-excited Auger spectroscopy.

The spectroscopic mode of STM works very well within a few electronvolts from the Fermi edge [3], but gives no access to core levels, being the 'fingerprint' of elements and their chemical environment in a compound. Energy-filtered TEM does give access to core levels via electron energy loss spectroscopy (EELS) yielding the electron loss near-edge structure. The performance of this technique is very high for specimens with good crystalline order being sufficiently thin to transmit the electron beam. 3D nanodevices can only be studied when thin samples are cut out exactly at the position of interest. For a fast control during a wafer production, chemical surface reactions on a catalyst, etc, spectroscopic TEM is not suitable. Obviously, there is still a strong need for other powerful tools for non-destructive chemical nanoanalysis of surfaces of thick specimens.

Looking at the problem with the eyes of a spectroscopist, we find x-ray induced photoelectron spectroscopy the most powerful technique, named electron spectroscopy for chemical analysis (ESCA). Established in the 1960s by Siegbahn *et al* [4], ESCA comprises x-ray photoemission spectroscopy (XPS) and x-ray excited Auger electron spectroscopy (AES). Characteristic x-ray lines (often Mg Kα at 1253.6 eV or Al Kα at 1486.6 eV) from water-cooled anodes (fixed or rotating) or monochromatized synchrotron radiation are used to excite photoelectrons and Auger electrons. Energy analysis of the electrons yields the core level binding energies. This facilitates a fingerprint-like detection of elements and their chemical states in compounds. Corresponding spectra of all elements (except H, He and the heavier transuranium elements) and many compounds have been tabulated (e.g. [5]). This makes the interpretation of spectra easy and reliable and allows for a quantitative analysis with reasonable accuracy down to 4–5 at.% [6]. It is near at hand that the combination of ESCA with microscopy provides an attractive surface analytical tool.

There have been several approaches to combine ESCA with lateral resolution. A straightforward way is to focus the x-ray beam in a small spot and scan the surface, taking spectra at each point. This concept is used in various laboratories (e.g. [7]) and in a commercial instrument [8]. The alternative way is parallel image acquisition via a magnifying lens system and an imaging energy analyser. This approach provides both a higher data acquisition rate and the possibility to take energy-filtered images at selected XPS lines and in real time.

Early commercial solutions [9–11] added an imaging lens to a hemispherical energy analyser; later designs [12–14] started from proven electron microscopes that were complemented by energy analysers with good imaging capabilities. A fully aberration corrected instrument is under construction and test [15].

In order to fully exploit the potential of ESCA in an electron microscope, the energy range accessible with Mg or Al Kα radiation should not be restricted. This poses a high challenge to the electron optical design because Liouville's theorem prevents feeding a large-solid-angle ensemble of electrons starting at 1.5 keV kinetic energy into an energy analyser operating at a pass energy of typically 100 eV or even less. In the present paper we describe a novel solution that attacks the problem of phase-space volume by aberration correction (α^2-term) of the analyser. This is accomplished by the antisymmetry of a tandem configuration of two hemispherical analysers. Besides elimination of the analyser's spherical aberration the tandem set-up largely retains the time structure of the electron signal, unlike a single hemisphere. This is an important feature for future energy- and time-resolved studies.

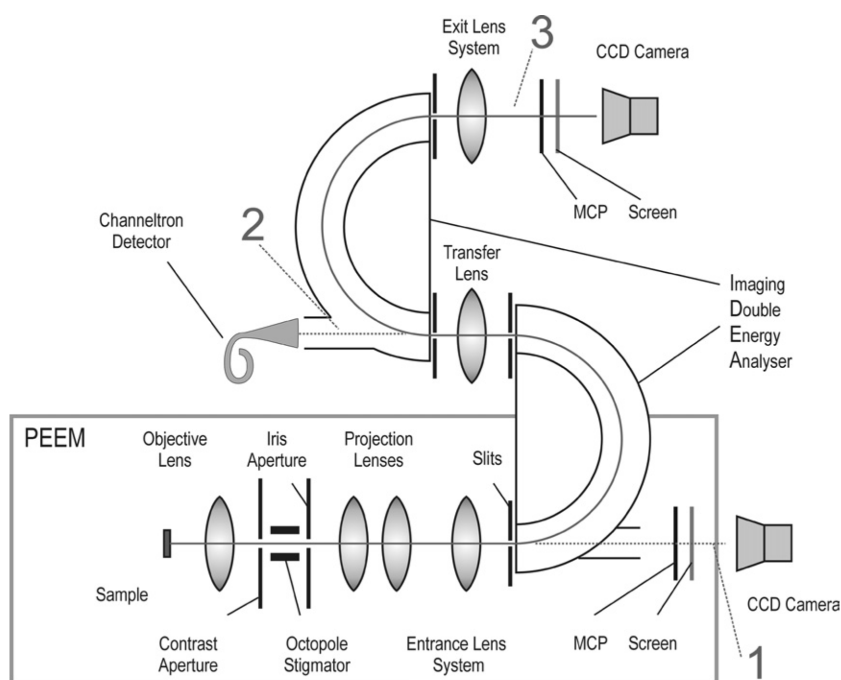

Figure 1. Schematic layout of the nanoESCA instrument. The three paths of the electrons are indicated: (1) PEEM-mode, (2) selected area spectroscopy, (3) energy-filtered ESCA imaging. The grey box envelops the elements of the PEEM mode.

2. Description of the instrument

2.1. Basic concept

The instrument developed—called NanoESCA—is derived from an electrostatic photoemission electron microscope (PEEM) column and a twin hemispherical energy analyser (HSA). Figure 1 shows a schematic view of the electron optical layout. The path of the electrons for the three modes of operation are indicated: (1) direct non-energy-filtered PEEM imaging, (2) selected area spectroscopy and (3) energy-filtered ESCA imaging for kinetic energies up to 1.6 keV.

The PEEM column is used as the entrance lens of the analyser. It consists of an immersion objective lens with exchangeable and adjustable contrast apertures, an electrostatic octopole stigmator and two projective lenses. A continuously adjustable iris aperture in the first intermediate image plane is used to select a defined field of view for selected area spectroscopy. The field of view can be chosen and defined in size and position using the direct PEEM imaging mode. The projective lenses are either used to project the first intermediate image onto the screen for direct non-energy-filtered imaging or to adapt the electron beam to the pass energy of the analyser.

The analyser of the nanoESCA (called the imaging double energy analyser, IDEA) is a new development [16] essentially consisting of two hemispherical analysers. The action of the two hemispheres is illustrated in figure 2. In the spherical electrostatic field, similarly to planetary motion (Kepler ellipses), the trajectories of the electrons coincide after a complete revolution, independent of the start energy and start angle, i.e. a perfect achromatic image without aberrations is generated. The second half of the elliptical orbit compensates the

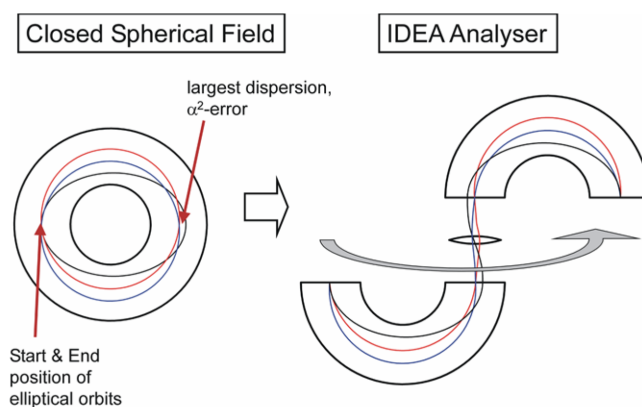

Figure 2. Schematic illustration of the basic design idea for the imaging double energy analyser. The different schematic particle trajectories are drawn for the same kinetic start energies.

aberrations of the first half. After 180° revolution the largest dispersion occurs. Here the energy selecting slit is placed. The problem of this—so far theoretical—model is the transport of electrons into and out of the inner and outer spheres, as they block the space for the entrance lens and the detector. To solve this task we divided the spherical field into two halves, mirrored the second and removed it from the first. A transfer lens images the electrons leaving the first hemisphere onto the entrance of the second hemisphere.

For selected area spectroscopy the deflection field of the second hemisphere is switched off. The electrons then are focused by the transfer lens into a channeltron detector. With this detector quantitative spectra suitable for ESCA analysis can be obtained, without the uncertainty of image conversion by the channelplate–screen–camera assembly.

The good lateral resolution of the microscope is accomplished by the immersion objective lens, which consists of a sample near ground potential and an extractor anode that is kept at up to 16 kV. The electrons decelerate towards the column, in contrast to other cathode lenses where the drift energy of the electrons in the column equals the extractor energy [17]. We found that the combined error due to spherical and chromatic aberrations can also be minimized for a column potential of about 8% of the extracting voltage. This has the advantage that for spectroscopic imaging a large part of the deceleration towards the analyser's pass energy is already done by the objective lens while maintaining the advantage of a high accelerating field with small aberrations. The theoretical resolution limit of our cathode lens is about 10 nm for non-energy-filtered threshold emission. We will show below that a low pass energy is an advantage for the imaging with good spatial and energy resolution and with high transmission. A typical pass energy for the nanoESCA instrument is 100 eV or below. For this pass energy a deceleration of about one order of magnitude via the projective lenses is sufficient, and this can be easily accomplished over a large range of magnifications.

2.2. Imaging mode: IDEA compared with HSA

The energy resolution of the IDEA analyser is defined by the slit at the exit of the first hemisphere and therefore is identical to the energy resolution of a single HSA with the same radius. The energy resolution ΔE at a pass energy E_{pass} of an HSA with mean path radius R can be written as

$$\Delta E = E_{\text{pass}} \left(\frac{d}{2R} + \alpha^2 \right), \tag{1}$$

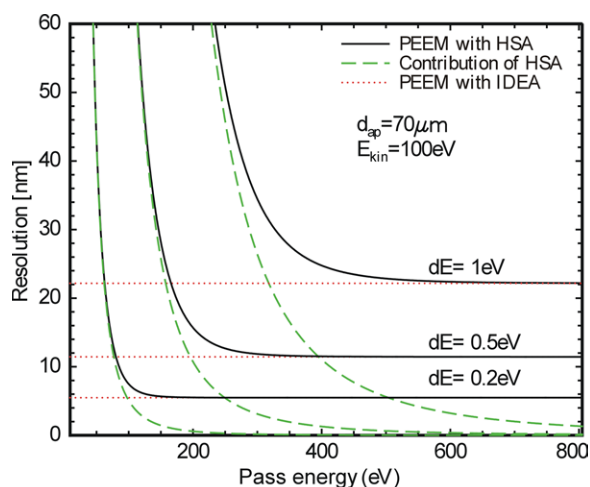

Figure 3. Calculated pass energy dependence of the lateral resolution of an energy-filtered image, comparing the nanoESCA with the HSA resolution at different energy resolutions dE. The starting energy is $E_{\text{kin}} = 100$ eV. The HSA contribution results from the α^2-term in equation (1).

where d is the slit width and α is the maximum angle of electrons with respect to the optical axis. The α^2-term can be regarded as the spherical aberration of the analyser's dispersion. A good energy resolution ΔE requires either a small pass energy E_{pass} or a small slit width d, providing the α^2-term is small enough. Which of the two terms should be minimized preferably can be decided by discussing the transmission of the system. Neglecting all higher order terms, the accepted phase space in dispersive direction at the entrance slit (or the linear transmission of the HSA) can be written with help of equation (1):

$$T_d \propto \sqrt{E_{\text{pass}}}\alpha d = \frac{\Delta E}{\sqrt{E_{\text{pass}}}}\alpha 2R. \qquad (2)$$

Assuming a constant aperture angle α at the analyser's entrance slit (in our configuration depending only on the contrast aperture size or the field of view), it can be seen that at a given energy resolution the transmission drops with increasing pass energies. This holds for configurations with a reciprocal image plane in the analyser's entrance as described by Tonner [12] and Coxon [9, 10] that have a coupling lens between the image plane in front of and behind the hemisphere and the entrance and exit slits. This lens maps an angular distribution in the image plane into real space coordinates at the entrance or exit plane of the analyser and vice versa. Calculating the transmission in the image plane, the coordinates can be transformed into the entrance plane of the analyser, and the focal lengths cancel out in the calculation.

We have calculated the contribution of an HSA analyser operated with coupling lenses to the image aberrations as a function of the pass energy and compared it to the IDEA that can be operated without or with coupling lenses. Assuming a spherical aberration of the coupling lenses, the analyser's transfer equation (1) gives rise to image aberrations through the α^2-term.

An example for a typical setting with a large contrast aperture (70 μm diameter) and a kinetic energy of 100 eV is shown in figure 3. Here the spherical aberration coefficient of the HSA's coupling lenses is $C_s = 250$ mm. The dotted curve shows that within this calculation the spatial resolution of the IDEA is independent of the pass energy. In terms of the chromatic aberrations the spatial resolution of the PEEM–IDEA combination is limited by

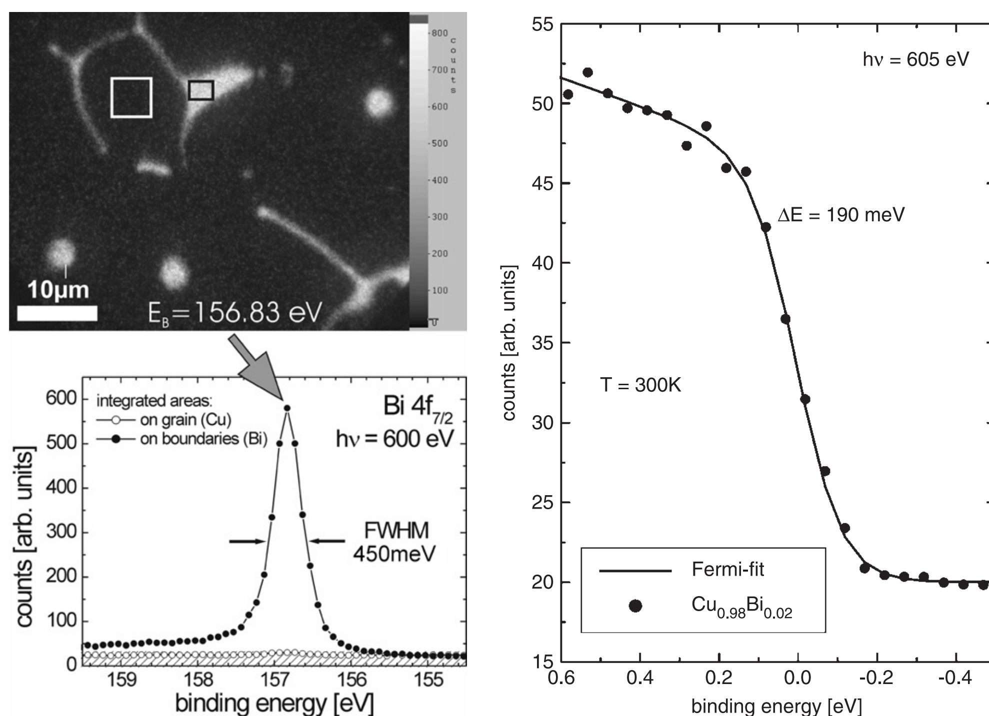

Figure 4. Spectroscopic investigations of a $Cu_{0.98}Bi_{0.02}$ polycrystal. The measurements were made with 50 eV pass energy and slits of 1 mm width. Left: imaging at the Bi $4f_{7/2}$ core-level on the grains (open dots) and on the grain boundaries (filled dots), visible bright in the Bi image. Right: Fermi edge of the same sample (dots). The analysis of the data leads to an analyser resolution of $\Delta E_{\mathrm{fwhm}} = 189$ meV (see the text).

the chromatic aberration of the PEEM lens. For a single hemispherical analyser with entrance and exit coupling lenses, the α^2 aberration blurs the image at low pass energies. Obviously this aberration is compensated in the IDEA configuration by the second hemisphere. For pass energies larger than 500 eV the effect becomes negligible. For high transmission a low pass energy is favourable, as we saw above. The correction of the spherical aberration of the dispersion achieved with IDEA analyser allows us to work in that region with good spatial resolution.

3. Results

3.1. Spectroscopic performance

As an example of the good spectroscopic performance we show measurements made on a $Cu_{0.98}Bi_{0.02}$ polycrystal [18]. The $Bi4f_{7/2}$ core level and the Fermi edge (figure 4) are detected using a photon energy of $h\nu = 600$ and 605 eV at the UE-52/SGM undulator micro-spot beamline [19] at BESSYII. The photon flux was 3×10^{12} photons mm^{-2} s^{-1} into a spot of about 300 μm FWHM as was measured with the nanoESCA. The pass energy of the analyser was 50 eV; the slit width at entrance and exit was 1 mm. The acquisition time for one image was 60 s, and it was 20 s for the Fermi-edge measurements. In an image series taken at binding energies around the Bi $4f_{7/2}$ XPS line (the upper left of figure 4 shows the image taken

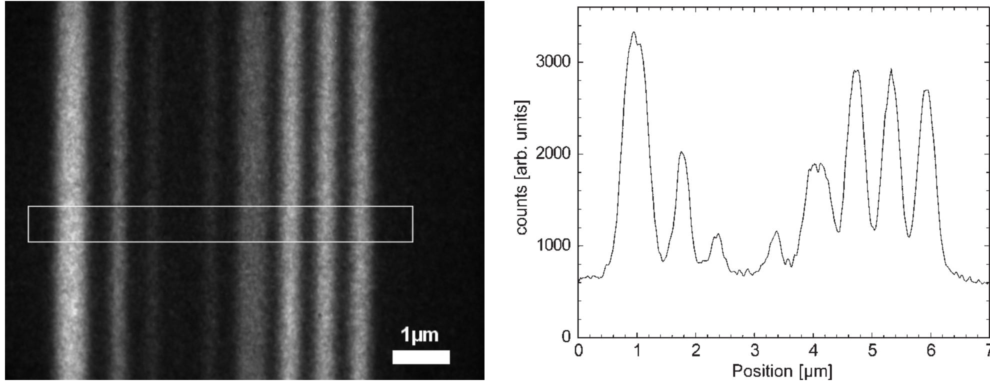

Figure 5. Left: GaAs/Al(0.65)Ga(0.35)As heterostructure imaged at the Al 2p core level ($h\nu = 120$ eV, pass energy 100 eV). Right: intensity profile over the area indicated on the left.

at $E_\mathrm{B} = 156.83$ eV) only the grain boundaries appear bright. The measurement shows the segregated Bi located in the grain boundaries of the Cu grains of the crystal whereas only very small Bi concentration is detected on the Cu grains themselves. This low background intensity demonstrates the capability of the instrument for spectroscopic imaging.

The measurement revealed that Bi segregates to the boundaries between the Cu grains of the crystal; no Bi concentration was detected on the Cu grains. This low background intensity demonstrates the capability of the instrument for spectroscopic imaging. In the image taken at the Bi $4\mathrm{f}_{7/2}$ XPS line (upper left), only the grain boundaries appear bright. The energy resolution of the measurements was determined by measuring the Fermi edge at room temperature. The measured energy width of $\Delta E_\mathrm{exp} = 230$ meV (12%–88% rise) consists of three intrinsic widths: the thermal width of the Fermi edge at room temperature (about $4k_\mathrm{B}T \approx 102$ meV), the photon bandwidth of the synchrotron beamline ($\Gamma_\mathrm{Ph} = 80$ meV, [20]), and the analyser's energy resolution ΔE. For simplicity, we fit the measured Fermi edge by an effective Fermi–Dirac distribution plus linear background. One of the fit parameters is a pseudo-temperature T_m which gives the experimental width $\Delta E_\mathrm{exp} = 4k_\mathrm{B}T_\mathrm{m}$ of the Fermi edge including thermal and instrumental broadenings. From this experimental width, the energy resolution can be extracted in a simple and sufficiently accurate way to be $\Delta E = \sqrt{(4k_\mathrm{B}T_\mathrm{m})^2 - \Gamma_\mathrm{Ph}^2 - (4k_\mathrm{B}T)^2} = 190$ meV [21]. This measured energy resolution is even better than the value calculated using equation (1), as the PEEM lens forms a virtual slit at the analyser's entrance which is smaller than 1 mm.

3.2. Spatial resolution with synchrotron excitation

As a test structure for the spatial resolution imaging electrons of an XPS line we used a $\mathrm{GaAs/Al_{0.65}Ga_{0.35}As}$ heterostructure [22]. The sample consists of alternating layers of different thicknesses that are cut and polished perpendicular to the layers. Before the measurement the sample was cleaned by Ar-ion sputtering. With an excitation energy of $h\nu = 120$ eV and about 10^{12} photons mm^{-2} s^{-1} we imaged the Al 2p core level at a kinetic energy of 44 eV. The pass energy of the analyser was 100 eV for these measurements. Figure 5 shows an image of the sample and an intensity scan across the area indicated. The acquisition time was 300 s.

The 500 nm wide line at the left-hand side gives a very high contrast of about 88% of the Al 2p-intensity with respect to the background intensity taken far away from the Al features.

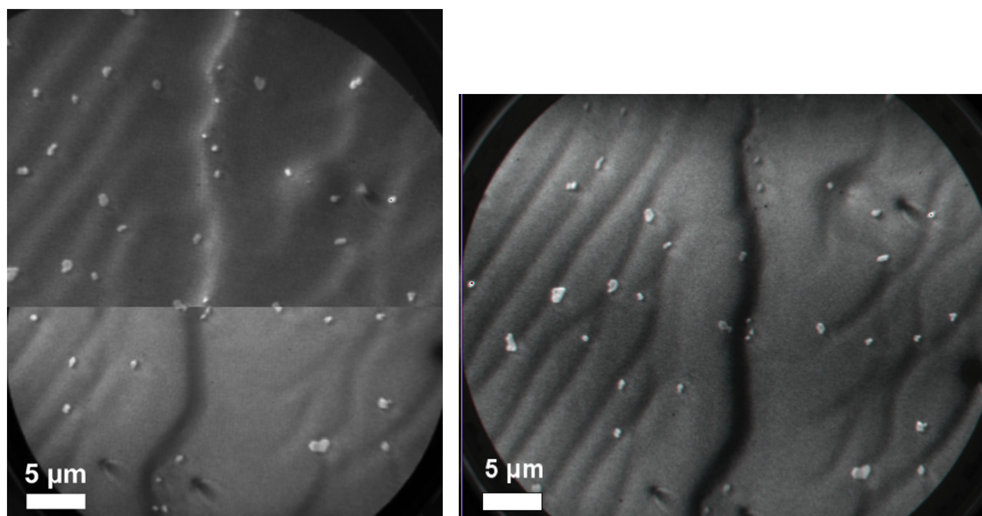

Figure 6. Ag crystallites on Si(111) imaged with direct PEEM mode (left) and energy-filtered imaging (right). The energy-filtered image shows no deterioration due to the energy filtering but a higher contrast. The PEEM image is assembled of two images with different contrast aperture positions. The image acquisition time was 6 s in both the energy-filtered and unfiltered modes.

Alternating 300 nm wide lines separated by 300 nm spaces, which appear at the right-hand side of the image, are resolved with a contrast of $58 \pm 3\%$ and an edge resolution of 120 nm (intensity rise from 16% to 84%). Isolated 50 nm wide lines are clearly distinguishable from the background intensity. The data have been taken with no vibrational damping of the instrument and therefore mechanical vibrations in the synchrotron environment are supposed to be the limiting factor for lateral resolution at the current state of development.

3.3. Comparison of energy-filtered and non-energy-filtered imaging

We compared the PEEM mode and the energy-filtered imaging mode using an Hg high-pressure UV lamp working in the threshold excitation regime. The sample was Ag crystallites on an Si(111) surface. Ag was deposited by e-beam evaporation on a clean Si(111) surface kept at elevated temperature (T about 500 K) *ex situ*. At the given conditions the Ag dots showed a width of typically some 100 nm to some microns. The size of the dots was calibrated using scanning electron microscopy (SEM) prior to the PEEM measurements.

Figure 6 shows a comparison of images taken in the two modes (1 and 3 in figure 1) with a comparable field of view. The Ag dots appear bright on the darker Si substrate. The Si substrate has no uniform intensity as seen with the SEM; a wide wavy line running from top to bottom of the images and some smaller lines running diagonally from the lower left side across the sample can be assigned to terrace edges corresponding to multi-atomic steps. The terrace edges appear bright or dark depending on position of the contrast aperture used. This is seen in the PEEM image that is combined from two images with different contrast aperture positions. Additionally the terrace edges are not imaged as sharply as the Ag dots. The local field at the edges is probably distorted by two effects: the topography of the edge and a different work function of the Si surface differing from the (111)-orientation. Consequently, the electron trajectories are bent and appear under a changed emission angle [23].

The energy-filtered image (figure 6, right) was taken at an analyser pass energy of 100 eV. The kinetic energy was set to give highest intensity in the Ag dots. The image has the same quality with respect to lateral resolution and distortion-free imaging as the unfiltered PEEM image. In the energy filtered mode the resolution for this sample was 80 nm. The contrast of the Ag dots to the background is enhanced by the energy filtering. This can be explained by a lower work function of the Ag dots. Optimizing the intensity of the Ag structure, a kinetic energy was chosen close to the spectrometer cut-off at the maximum of the photoelectron distribution. Assuming a higher work function of the Si substrate, the Si appears darker as its emission lies within the spectrometer cut-off region due to the different work function. In our case it is not possible to assign definite work function differences to the surfaces imaged as they were not atomically clean due to the *ex situ* preparation. In general it is easily possible to study quantitatively work function differences and image structure using this contrast mechanism even with threshold emission.

4. Conclusions

A novel approach for imaging ESCA with lateral resolution in the 100 nm range was described. In order to be compatible with the widely used Mg and Al Kα laboratory x-ray sources delivering photon energies of 1253.6 and 1486.6 eV, respectively, the useable kinetic energy range extends up to 1.6 keV. At such high kinetic energies, the conservation of phase-space volume (Liouville's theorem) is a serious electron optical problem. Retardation of an electron beamlet starting at 1.5 keV kinetic energy to a typical analyser pass energy of 100 eV results in an enhancement of the angular divergence by almost a factor of 4 (at constant magnification). This, in turn, deteriorates the energy resolution and imaging quality of a hemispherical analyser. Thus, the angular divergence needs to be restricted by an aperture stop in the reciprocal image plane, leading to a strong reduction of intensity. In the present tandem configuration this α^2-term of the spherical aberration of the analyser is eliminated due to the antisymmetry of the tandem configuration of two identical analysers.

The entrance lens is based on an electrostatic photoemission electron microscope column with integrated sample stage. A standard sample holder (OMICRON type) facilitates easy and fast sample exchange. Non-energy-filtered PEEM imaging is easily accomplished by switching off the analyser potentials ('straight-through-mode'). Another mode of operation is selected-area microspectroscopy, facilitated by switching off the second hemispherical analyser and using a channeltron electron detector behind the exit of the first analyser.

First test operation of the instrument employed synchrotron radiation at the UE-52/SGM Undulator beamline at BESSY II. An analyser resolution of 190 meV has been determined at a photon energy of 605 eV.[5] The spatial resolution has been measured using a semiconductor heterostructure yielding an edge resolution of 120 nm. Both values will certainly be improved in the future by more optimized settings of the electron optics and by eliminating mechanical vibrations. The imaging quality of the analyser has been tested in threshold photoemission using a Hg high-pressure UV lamp. Ag crystallites on Si(111) grown by e-beam deposition at elevated temperature showed a higher contrast and no reduction in lateral resolution in the energy-filtered images as compared to the non-filtered image of the same sample position. This result ensured that no visible image deterioration and no distortion occurred upon energy filtering.

Besides its capability of energy-resolved imaging on a selected XPS-line (imaging ESCA), the instrument strongly improves the resolution in synchrotron-radiation-based X-PEEM. This

[5] Recently, an energy resolution of 110 meV (12%–88% rise) has been reached at 80 keV kinetic energy in the soft x-ray range.

is a consequence of a strong reduction of the chromatic aberration of the imaging optics (essentially the electrostatic extractor field) by selecting a narrow energy interval of electrons forming the image. Usually, very small aperture stops in the back focal plane of the objective lens have to be used to minimize the chromatic aberration. However, this dramatically reduces the intensity [24, 25]. Last but not least, the antisymmetric tandem configuration largely compensates the deterioration of time-resolution of the electron signal. In a single hemisphere the differences in transit time of the outer and inner ray paths are substantial and prevent time resolutions in the sub-nanosecond range. As the outer and inner paths are reversed when passing the second hemisphere, these different transit times cancel out in first approximation. This will allow energy- and time-resolved detection, e.g. using a delayline detector [26] for image acquisition.

Acknowledgments

The $Cu_{0.98}Bi_{0.02}$ samples were prepared by M Ziehmer and C Krill III from the Universität des Saarlandes, FR 7.3 Technische Physik. The authors wish to thank the BESSY staff, especially F Senf for his help with the beamline. Part of this work has been funded by the German government (BMBF, grant FKZ-No. 13N7863, 13N7864, 13N7865 & 13N7847) and also by Deutsche Forschungsgemeinschaft (SFB 277).

References

[1] Haider M *et al* 1998 *Nature* **392** 768
[2] Rose H 1999 *Ultramicroscopy* **78** 13
[3] de la Broise X *et al* 2000 *Appl. Phys. Lett.* **76** 3142
[4] Siegbahn K *et al* 1967 *ESCA—Atomic, Molecular and Solid State Structure Studied by Means of Electron Spectroscopy* (Uppsala: Almquist and Wiksell)
[5] NIST XPS-Database, http://srdata.nist.gov/xps/
[6] Powell C J and Seah M P 1990 *J. Vac. Sci. Technol.* A **8** 735
Seah M P 1995 *J. Electron Spectrosc. Relat. Phenom.* **71** 191
[7] Thieme J, Rudolph D, Schmahl G and Umbach E (ed) 1996 *X-Ray Microscopy and Spectromicroscopy* (Berlin: Springer)
[8] Quantera SXM, product information, Physical Electronics (ULVAC-PHI)
[9] Coxon P *et al* 1990 *J. Electron Spectrosc. Relat. Phenom.* **52** 821
[10] Wardell I and Coxon P 1991 *European Patent* EP0246841B1
[11] Axis Ultra, product information, Kratos Analytical (Shimadzu), Manchester (UK)
[12] Tonner B P *et al* 1997 *J. Electron Spectrosc. Relat. Phenom.* **84** 211
[13] Bauer E 2001 *J. Electron Spectrosc. Relat. Phenom.* **114–116** 975
[14] Imaging Energy Analyser, product information, Elmitec, Clausthal-Zellerfeld (Germany)
[15] Fink R *et al* 1997 *J. Electron Spectrosc. Relat. Phenom.* **84** 231
[16] Patent pending
[17] Chmelik J, Veneklasen L and Marx G 1989 *Optik* **83** 155–60
[18] Schmidt S *et al* 2003 *Bessy Annual Report*
[19] Peatman W B *et al* 1995 *Rev. Sci. Instrum.* **66** 2801–6
[20] Petersen H *et al* 1995 *Rev. Sci. Instrum.* **66** 1777–9
Senf F *et al BESSY Users Info UE52-SGM*
[21] Greber T, Kreutz T J and Osterwalder J 1997 *Phys. Rev. Lett.* **79** 4465–8
[22] Sample BAM-L002 *Nanoscale Strip Pattern for Length Calibration and Testing of Lateral Resolution* (Berlin: Bundesanstalt für Materialforschung (BAM))
[23] Nepijko S A *et al* 2000 *J. Microsc.* **199** 124–9
[24] Anders S *et al* 1999 *Rev. Sci. Instrum.* **70** 3973
[25] Liebl H 1988 *Optik* **80** 4
[26] Oelsner A *et al* 2001 *Rev. Sci. Instrum.* **72** 3968